

# Fault Scarp Detection and Attribute Analysis Using High-Resolution Satellite Imagery and LiDAR in Earthquake-Prone Areas

OKUJAGU, D. C<sup>1</sup> and Oghonyon R.<sup>2</sup>

<sup>1&2</sup>Department of Geology, University of Port Harcourt, Nigeria

Email: diepiriye.okujagu@uniport.edu.ng

Corresponding Authors Mail: rorome.oghonyon@uniport.edu.ng

---

## Abstract

Fault scarps are structural terrace that are defined by subsurface structural deformation of rocks that are triggered by Earth movements of tectonic activities. They serve as critical indicators of geologic hazards following earthquakes, offering valuable insights into active crustal deformation. Despite extensive ground-based surveys, numerous uninvestigated faults remain in regions surrounding known active faults, particularly in earthquake-prone areas. This imperative for advanced remote sensing techniques to improve fault scarp detection and analysis. The primary objective of this study is to develop an algorithm that leverages morphological attributes derived from variance edge, high-resolution satellite imagery and LiDAR data using machine learning methods as quick insights for structural analysis. Additionally, the study aims to integrate geometric aspects of registered optical imagery and LiDAR data into a unified framework for enhanced fault scarp identification and delineation. Our approach involves the adaptive combination of geometric attributes to address challenges in detecting and analyzing fault scarps in complex terrains for geological significance and for the benefit of mankind. Study areas were selected in the central part of Myanmar, a region characterized by active fault systems. Results demonstrate an overall accuracy of approximately 80% in fault scarp detection, highlighting the effectiveness of the proposed methodology. These findings have significant implications for improving earthquake hazard assessments and disaster preparedness in vulnerable regions in this period of changing climate.

**Keywords:** fault scarp, active fault, earthquake, very high resolution, LiDAR, Earth Observation, Python, morphological Attribute Profile Shapes

---

Date of Submission: 24-04-2025

Date of acceptance: 04-05-2025

---

## I. INTRODUCTION TO FAULT SCARPS

Fault scarps are created by tensional stress effects within the rock mass. The structural deformation within sections of the rock in areas of weak bonding creates zones of displacement of the fault blocks. Thereby, creating openings within the rocks, fault throws and faults planes resulting to the fault scarp. Active fault detection is critical for the assessment of seismic hazards formed by the release of seismic waves (body and surface waves) at depth. The recently developed technology of high-resolution satellite imagery provides an excellent platform to ascertain the fault scarp (or escarpment) for active fault recognition around the world. The advantage of satellite images lies in their broad coverage, which cannot be matched by airborne sensors at similar resolution quality (ELLIOTT, 2022). This technology, combined with traditional field inspection and the LiDAR approach, offers additional benefits such as low cost effect, no terrain restrictions and short data acquisition times, complementing traditional fault investigation techniques (Wei et al., 2021). Recognition of fault scarps through high-resolution satellite imagery can generate far more fault information in a timely manner (Figure 1), further improving seismic hazard assessment and engineering-project planning (Zou et al., 2021).

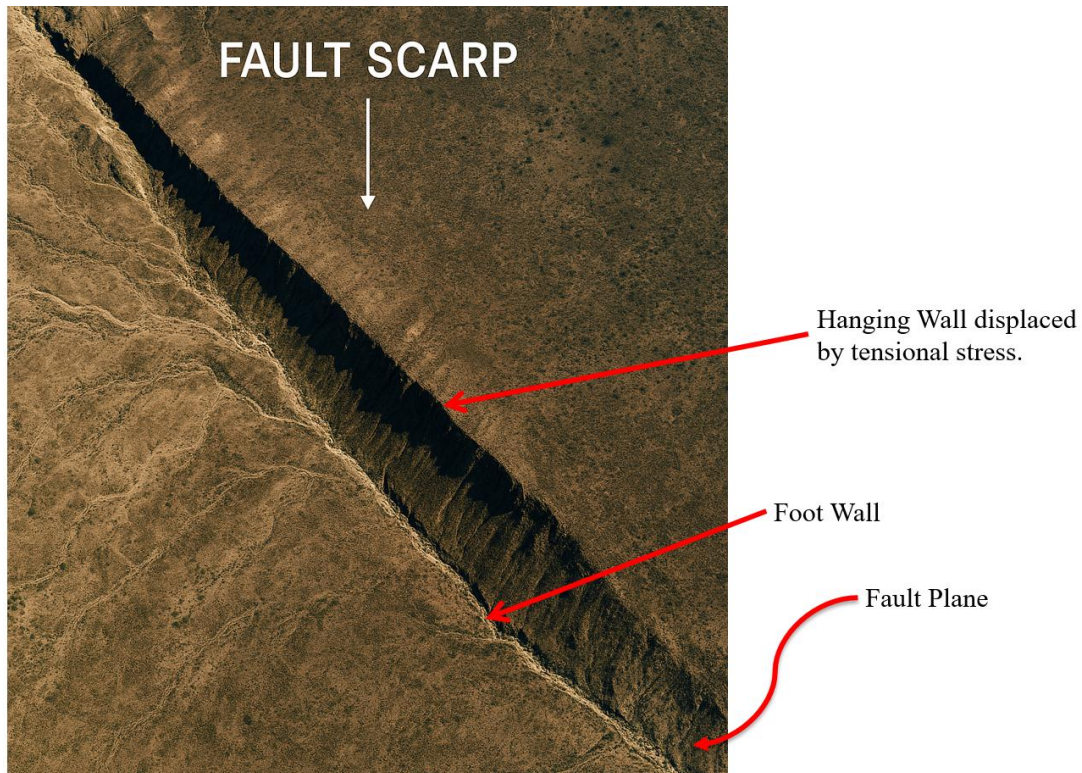


Figure 1: Example of fault scarp identification using high-resolution satellite imagery.

Indeed, earthquakes are considered the most frightening of all natural disasters (Figure 2). These disasters have struck and shattered many cities around the world from ancient times to the present, with the reverberation of earthquake-induced destruction frequently forcing changes in the evolutionary trajectory of impacted civilizations (Mozaffari et al., 2024). The formation of active fault plateaus (or horst-graben) beneath the Earth's surface, combined with the complex energy release during earthquakes, makes predicting the next rupture event a difficult task (Guo et al., 2022). To guide feasibility studies for large project investments worldwide, well-studied databases that provide detailed fault parameters are essential. There is an urgent need to expand current fault information to enhance seismic hazard assessments for rapidly growing structures, dams, railway networks, and nuclear plants (Nilofar & Lazarova-Molnar, 2023). These facilities, built for the convenience of people and the advancement of human civilization, face potential rupture hazards beyond the scope of recorded history. The severity of disasters caused by future earthquake events may far exceed the risk estimations of invested projects (Berghout & Benbouzid, 2023).

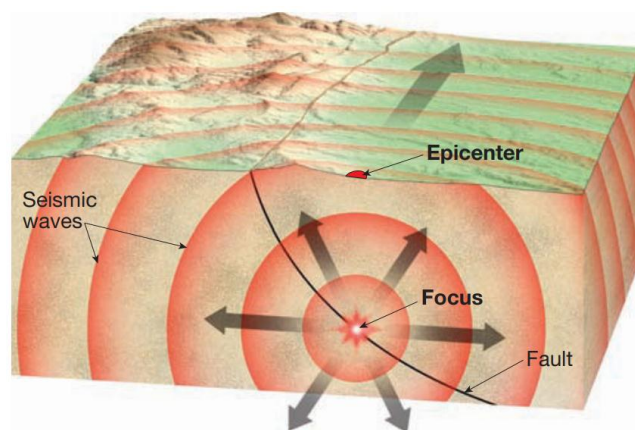


Figure 2: Schematic representation of Earthquake focus, epicenter and associated seismic risks (adapted from Frederick Edward, 2012).

### 1.1. Definition and Characteristics of Fault Scarps

The term "fault scarp" is frequently used in the geoscience literature (Figure 3). The word "scarp" refers to a small line of cliffs as it occurs in English; however, in French, it is equivalent to "escarpement," and "scarp" would be accurately translated into "écart." Therefore, it may be more appropriate to use the term "cliff." As it is used in other languages, the expression "fault cliff," which identifies the geological phenomenon, appears appropriate indeed. Culling from the meaning, a "fault" refers to a discontinuity in the rock mass across which displacement has occurred, and "displacement" refers to the relative movement of prominent rock units on either side of the fault (Chiarella et al., 2021; Chiama et al., 2023).

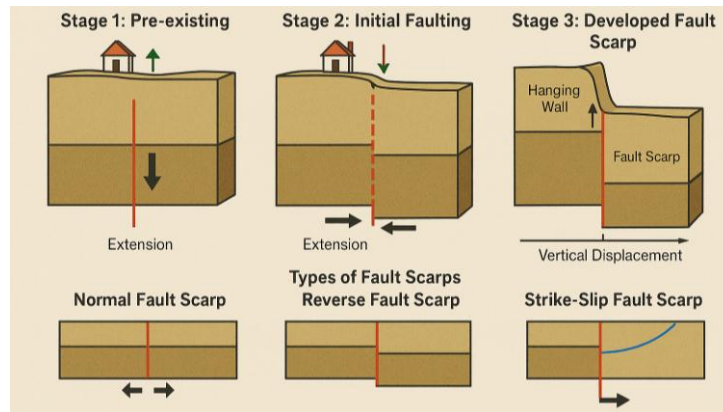


Figure 3: Schematic representation of fault scarps and their formation

Details derived from the examination of active tectonic features, such as fault scarps, represent initial steps in studying the origin of the catastrophic potential of specific active faults. These features serve as the main surface expression of active faults resulting from elastic rebound associated with underlying fault movement (Figure 3). They provide significant control on engineering applications, including borehole positioning, construction planning, groundwater flow, earthquake potential evaluation, and seismic hazard assessment (Holtmann et al., 2023). During an earthquake, a rupture occurs on a fault in the Earth's crust, causing displacement along both sides of the dislocation (Figures 2 and 3). This dislocation can open or close the Earth's surface, generating a rupture scarp or a vent. These ruptures are known as "earthquake fault scarps." Depending on the seismic wave energy of the earthquake, this scarp creation can vary in significance. However, it suffices to say that large and powerful earthquakes always generate significant earthquake fault scarps (Li et al., 2022; Ha et al., 2022).

## II. Remote Sensing and Fault Scarp Detection

Remotely sensed data sources and methods, including satellite imagery, LiDAR, and detection algorithms, can provide robust and cost-effective techniques to map fault scarp geomorphology, including scarplet distribution, scarp and core (Table 1). Landslide studies have developed detection methods and tools based on digital elevation model (DEM) hillshading and contouring methods (Silva-Fragoso et al., 2024). Detailed mapping can improve understanding of earthquake history, scarplet segmentation, scarp age, and long-term slip rates (Table 1). However, thus far, these methods have been underused in fault scarp studies. LiDAR has notable advantages, including the ability to differentiate small details such as scarps, micro-ridges, and micro-faults from underlying ground morphology (Jamšek et al., 2024). The most detailed studies have utilized LiDAR in research on active faults (Zou et al., 2022).

Table 1: Summary of very high-resolution satellite systems used in fault scarp studies

Satellite System	Operator/Provider	Spatial Resolution (Panchromatic)	Revisit Time	Key Features/Capabilities	Applications in Fault Scarp Studies	Advantages / Additional Notes
WorldView-3	Maxar Technologies	0.31 m	~1 day (constellation)	Multi-spectral/SWIR bands, stereo imaging, high agility	High-resolution DEM/DSM generation; precise vertical offset measurements; tectonic geomorphology analysis	Best-in-class resolution; multispectral bands aid lithological/vegetation differentiation; supports fine-scale analysis.

<b>WorldView-4 (Legion)</b>	Maxar Technologies	0.31 m	~1 day (constellation)	Stereo imaging, high agility	Active fault mapping; high-precision DEM generation	Optimized for rapid tasking; critical for time-sensitive post-seismic studies.
<b>GeoEye-1</b>	Maxar Technologies	0.41–0.46 m	~3 days	High geolocation accuracy, multi-spectral data, stereo imaging	Paleoseismic analysis; detection of subtle topographic changes; GIS integration for fault mapping	High radiometric resolution improves surface contrast; reliable for DEM generation.
<b>Pléiades-1A/1B</b>	Airbus Defence & Space	0.50 m	~1 day (twin satellites)	Agile stereo acquisition, rapid revisit	3D fault analysis via stereo-pair DEMs; surface rupture mapping; post-seismic deformation monitoring	Rapid revisit supports temporal monitoring; high geometric accuracy for image co-registration.
<b>Pléiades Neo</b>	Airbus Defence & Space	0.30 m	~1 day (twin satellites)	Very high agility, stereo imaging	Ultra-detailed scarp mapping; high-resolution DEM generation	Improved resolution and agility over earlier Pléiades systems; ideal for dynamic fault zones.
<b>SPOT-6/7</b>	Airbus Defence & Space	1.5 m	~2–3 days	Wide swath (60 km), multi-spectral bands	Regional fault mapping; landscape evolution analysis; identifying lineaments in tectonic contexts	Wide coverage balances resolution and scale; cost-effective for regional tectonic studies.
<b>QuickBird (historical)</b>	Maxar Technologies (decommissioned)	0.61–0.65 m	~1–6 days	Historical archive data, multi-spectral bands	Retrospective fault evolution analysis; long-term change detection; erosion pattern assessment	Long imagery archive (2001–2015); cost-effective for historical baseline comparisons.
<b>IKONOS (historical)</b>	Maxar Technologies (decommissioned)	0.82 m	~3–5 days	Pioneering VHR, stereo imaging	Baseline studies for long-term fault activity comparisons	Early VHR system (1999–2015); foundational for modern fault scarp mapping techniques.
<b>SkySat Constellation</b>	Planet	0.50–0.72 m	Multiple daily passes	High revisit capability, stereo imaging possible	Scarp mapping; DEM generation; monitoring temporal changes	Frequent revisits enable near-real-time monitoring; affordable for academic use.
<b>KOMPSAT-3/3A/5</b>	KARI (South Korea)	Sub-meter (Optical & SAR)	~3–5 days (optical)	Stereo imaging (optical), SAR interferometry	DEM generation (optical); surface deformation monitoring (SAR)	Combines optical and SAR capabilities; useful for vegetated or cloudy regions.
<b>Cartosat-3</b>	ISRO (India)	0.25–1.0 m	~5 days	High-quality stereo capability (e.g., Cartosat-1 for DEMs)	Regional DEM generation for tectonic context; large-area fault studies	Strong stereo imaging for accurate DEMs; cost-effective for large-area surveys.
<b>Sentinel-2A/2B</b>	ESA	10 m (visible/NIR)	~5 days (combined)	Free/open-access, wide swath (290 km), multispectral	Regional fault studies; vegetation/soil moisture anomaly detection	Free data ideal for long-term or budget-constrained projects; wide swath covers

					(supports fault zone characterization)	extensive fault systems.
<b>ALOS PRISM/AVNI R-2</b>	JAXA (Japan)	2.5 m (panchromatic)	~46 days	Stereo photogrammetry, multi-spectral data, vegetated area penetration	Retrospective DEM generation; topographic displacement measurements	SAR data penetrates vegetation; archived data supports historical deformation analysis.

The advent of Global Navigation Satellite Systems (GNSS), such as CBERS, Landsat, ASTER, SPOT, IKONOS, QuickBird, WorldView, Airborne Laser Scanning (ALS), and LiDAR, along with digital aerial imagery, has also been employed to map fault scarps with varying degrees of success. The study of pre- and post-seismic high-resolution satellite imagery has the potential to delineate scarplets and reveal temporary earthquake features, such as liquefaction, rockfalls, ridge dislocations, fissuring, and faulting (ELLIOTT, 2022). These features can either contribute to the scarp deformation record or provide reconnaissance for ground-truthing studies in regions inaccessible to field researchers (Holtmann et al., 2023). Data from very high-resolution satellite systems that have been used in fault scarp studies are summarized in Table 1. Each system has unique advantages and disadvantages, and the trade-off between cost-effectiveness, resolution, scale, and ease of access to imagery must be balanced depending on the nature of the fault being studied and the research questions posed (Figure 4). The automatic detection of surface ruptures from very high spatial resolution (VHSR) satellite images has also shown promising results (Wang et al., 2021).

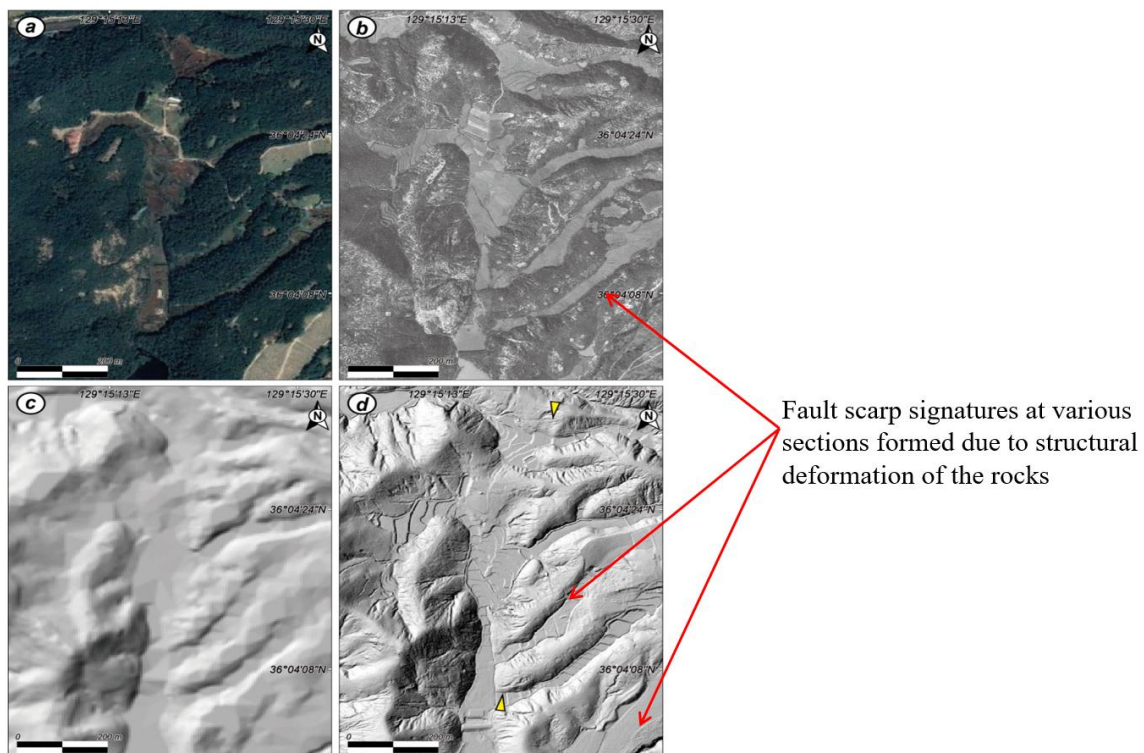


**Figure 4: Example of fault scarp delineation using LiDAR and VHSR satellite imagery (adapted from Ha & Seong, 2022).** Resolution comparison of various remote sensing technologies for the same area. (a) Google Earth Pro satellite image. (b) Aerial photography (1970s). (c) Hillshade using 1:5000 digital topographic maps (5 m resolution). (d) High-resolution LiDAR image hillshade. The yellow arrow indicates a fault scarp which was not observed in other images (0.5 m resolution).

### 2.1. Overview of Remote Sensing Technologies

Remote sensing taps the energy emitted or reflected by the planet and can be conducted either by means of surface sensors and aerial techniques or by using satellite systems. Surface sensors for terrain analysis may include photogrammetry for image creation, Structure from Motion (SfM), and several techniques for image and point cloud manipulation and analysis (Eskandari et al., 2023). In turn, ambient and satellite remote sensing are divided mainly into two approaches: passive and active. The spectral signature extracted, captured, and recorded

by passive remote sensors renders an image with the electromagnetic signatures of the Earth's surface (Figures 4 and 5). However, in active remote sensing, radar backscattering provides data on surface roughness and is readily available at different stages of an earthquake's aftermath (Jaud et al., 2022). Yet, none of these data sources can independently verify the real creation of post-earthquake surface displacement features such as those analyzed by LiSRA-wMHz (Lunina et al., 2024).

Most aerial photographs, corroborated by satellite Earth Observation (EO) images, post-earthquake surface slip estimates, and associated displacement fields, present very high resolution (between 0.5 to 2 meters for 85% of the images) and are excellent tools for geographical, physical, and environmental impact studies (Atwood & West, 2022). Nevertheless, very-high-resolution satellite imagery (VHRSI), with sub-metric resolution or smaller (Figures 4 and 5), is now suggested for tectonic and other surveying applications. VHRSI, particularly WorldView-3 and WorldView-4 data, has proven useful for observing micro-geomorphological defects and the smallest fault scarps on dry sea and playa beds (Wang et al., 2022).

## **2.2. Use of High-Resolution Satellite Imagery for Fault Scarp Identification**

The past decade has witnessed the commercial availability of increasingly high-resolution satellite imagery and the growing ease of access to these images (Chen et al., 2023). Increased spatial resolution in commercial satellite imagery provides enhanced detail in the spatial information returned, allowing for improved identification and analysis of fault scarps (ELLIOTT, 2022). Early identification of near-surface deformation has the potential to quickly assess the impact of an earthquake on assets, prioritize aid response, and mitigate risks to infrastructure systems (Holtmann et al., 2023). This high-resolution imagery offers the potential to create widely available, high-quality, authoritative, and up-to-date information about the location, extent, and degree of damage caused by earthquakes, as well as the effects of fault scarps (Wei et al., 2021).

Topographic features are visible in high-resolution panchromatic images, leading to good image quality even without multispectral data (Ha et al., 2022). Examples of high-resolution satellite sensors include WorldView-1/2/3/4, GeoEye-1, Ikonos, Pleiades, QuickBird, and SkySat. The form and spatial arrangement of a scarp influence how it is imaged and the directions in which it can be traced. High-resolution satellite images, due to their close-to-nadir viewing angles and narrow fields of view, can accurately represent small to medium fault scarps (elevation between 2 and 10 m) (Vega- Ramírez et al., 2021). Thus, satellite images offer the potential to monitor seismogenic activity and provide valuable information about current tectonic processes (Lu et al., 2022).

## **2.3. Challenges and Limitations in Remote Sensing of Fault Scarps**

The direct mapping of active faults is typically conducted using methods of ground surveying and field geology, as well as geophysical techniques such as tectonic geomorphology and ground physics (Ahmadi & Pekkan, 2021). Despite significant progress, traditional methods face numerous challenges in comprehensively studying these features in remote areas due to inaccessibility, dense highland vegetation, avalanche fans, and talus slope deposits, which hinder the identification of individual active components of fault zones in the field (Zanutta et al., 2020). In cases involving cross-scarp slopes, measuring the dip of the fault trace at sufficient points becomes even more difficult or impossible. Consequently, the topic of remote monitoring of displacement along fractures has become increasingly urgent (Figure 5), including mapping the morphogenesis and overall characteristics of fault scarps, ground cracks, slope failures, and cuts, as well as developing methods for detecting new small-scale ground ruptures in active tectonic areas (Styron & Pagani, 2020).

Experts widely use remote sensing techniques, as optical remote sensing images facilitate the determination of fault scarp features with greater accuracy (Deliry & Avdan, 2021). However, the effectiveness of remote sensing images is limited by the high temporal and spatial variability of the Earth's surface, which can obscure critical details (Natawidjaja et al., 2021).

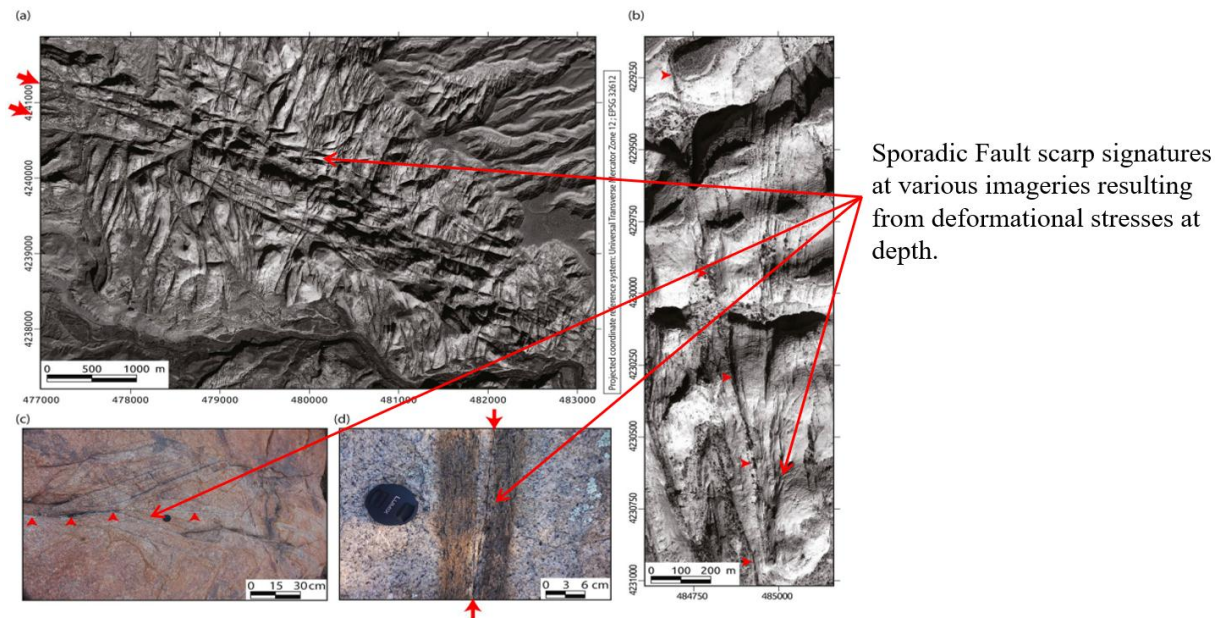


**Figure 5: Example of fault scarp mapping using optical remote sensing techniques (adapted from Mattéo, *et al.*, 2021).** Optical images of fault traces at ground surface, at different scales. Fault traces appear as dark lineaments in images, forming dense networks. At all scales, more pronounced, master fault traces (red arrows, not exhaustive) are “surrounded” (on one or both sides) by dense networks of closely spaced secondary faults and fractures of various lengths, generally oblique to and splaying off the master fault trace. (a and b) Pléiades satellite images of Waterpocket region, USA (ID in data statement). Two fault families are observed on (a), trending  $\sim$ NNE-SSW and  $\sim$ WNW-ESE. In both images, some of the faults have a vertical component of slip and thus form topographic escarpments that are seen through the shadows they form. (c and d) hand-held camera ground images in Granite Dells, USA; in (c) secondary faults splay from the underlined master trace, forming a fan at its tip; in (d), the underlined master fault trace is flanked on either sides by a narrow zone of intense fracturing, generally referred to as inner damage. Note the color change across the densely fractured inner damage zone (Figure 5).

### 3. LiDAR Technology and Fault Scarp Analysis

Currently, LiDAR (Light Detection and Ranging) technology is able to provide high-resolution topographic data and has developed into an essential tool for both terrain surface mapping and surface deformation detection (Schlöggl *et al.*, 2022). Although the technological methodologies and equipment used in LiDAR continue to evolve, the general methods remain consistent, and the applications of LiDAR in surface deformation extraction and detection are well-established (Kaartinen *et al.*, 2022). Combined with high-resolution satellite imagery (Figures 5 and 6), we aim to understand the interactions at each fault and its corresponding characteristics to clarify the true nature of faulting (Fitrah *et al.*, 2024). This approach should provide valuable data for earth scientists studying earthquake hazards, dynamic processes, structural associations, and faulting mechanisms in earthquake-prone regions (Ha *et al.*, 2022).

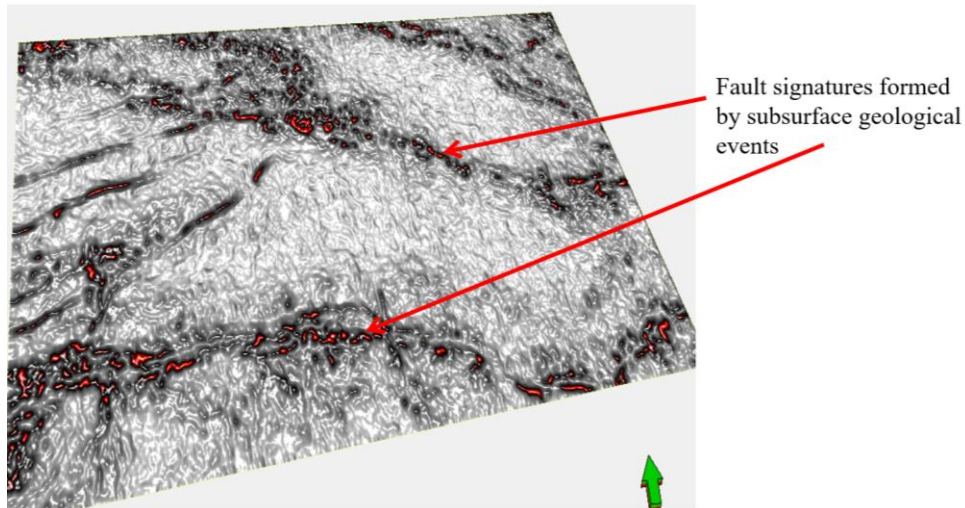


**Figure 6: Fault planes formed in association with deformational events at depth shown on variance edge attribute.**

The tectonics of active faults are of great concern due to their differential vertical offsets caused by repeated slip along the fault. The geometric characteristics of such features, including step-overs, bends, and en-echelon structures, have been validated in similar studies (Dembo et al., 2021). The asymmetric nature of these earthquakes is connected to earthquake asperities, which are directly linked to the material properties of the fault area (Figures 6 and 7). For instance, the low friction of slowly slipping patches near the trench and the slow slip to the southwest of the mainshock hypocenter resulted in larger coseismic deformation to the east of the mainshock (Shen et al., 2022). However, principal components (PCs) overlap with both coseismic and post-seismic slip, making it difficult to distinguish their respective contributions to GPS offsets (Rodriguez Padilla, 2023). Field-based observations in this area have been limited, complicating efforts to define future correlations with earthquakes (Figure 7). Additionally, a detailed and systematic study of such structural features and seismological characteristics remains lacking, particularly in areas affected by multiple earthquakes with adjacent underlying and near-surface structures (Xu et al., 2024).

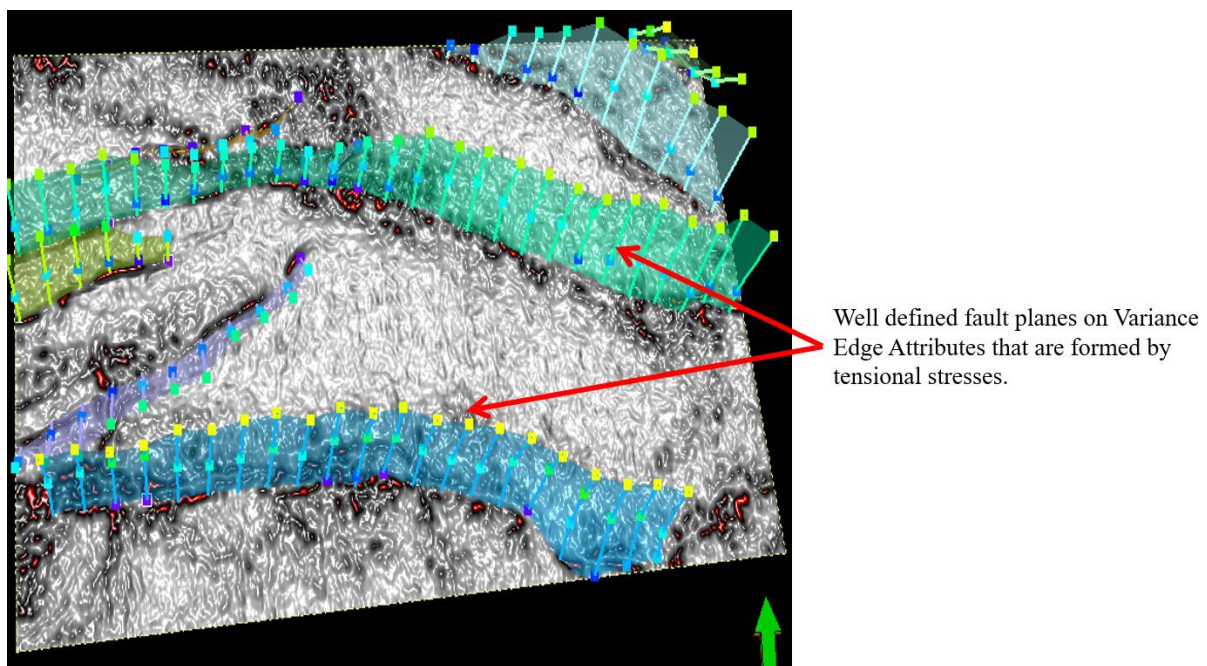


**Figure 7: Fault pillars created by deformational events at depth within the rock mass.**

### 3.1. Principles and Applications of LiDAR Technology

LiDAR, which stands for Light Detection and Ranging, is an airborne remote sensing technology that uses laser light to measure vegetation and ground surfaces beneath tree canopies (Shafapourtehrany et al., 2023). LiDAR data largely consist of X, Y, and Z coordinate measurements of discrete points. Light pulses emitted from the LiDAR hardware (laser source, scanner, and receiver) are partially absorbed by the tree canopy and scattered in various directions (Figure 8). Those returns that reach the surface are referred to as ground points. LiDAR hardware measures both the time difference between sending and receiving the return and the position of the LiDAR sensor at the time of the return. With knowledge of the positive direction of the scanner, the outgoing pulse, and various other factors, the resulting X, Y, and Z measurements of the returns may be projected to the ground surface (Jia et al., 2024).

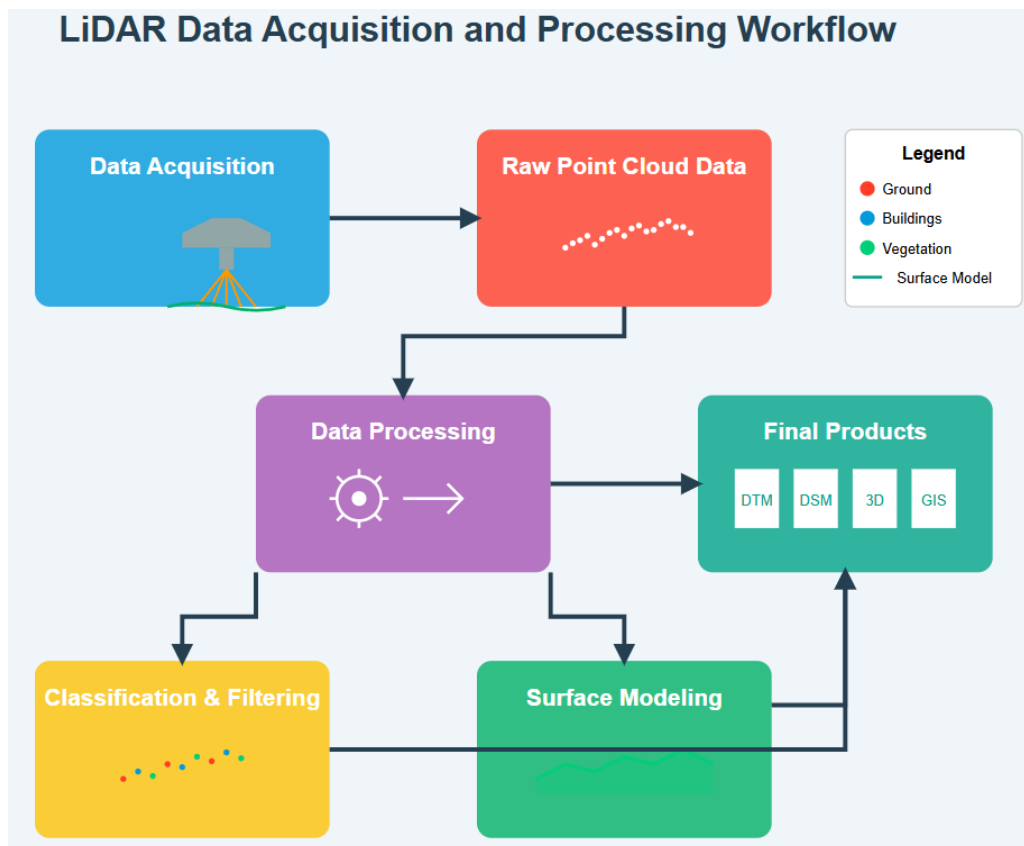


**Figure 8: Schematic representation of LiDAR data acquisition and processing (adapted from Shafapourtehrany et al., 2023).**

LiDAR has become a widely used technology in geological studies due to its extremely high spatial resolution and accuracy (Silva-Fragoso et al., 2024). It has opened various paths for quantitative geomorphology and been adopted for diverse applications, including fault scarp recognition, structure detection, mass movement monitoring, and faulting sea and continental cliffs (Jamšek et al., 2024). Additionally, through high-resolution topographic data extraction, high-accuracy point-based 3D imaging methods constitute a novel means for dynamic geological studies and can provide full 3D views of investigated topics, boosting the speed and clarity of specific detailed object analysis (Sercombe et al., 2023). This summary highlights the great potential of LiDAR. As the hardware evolves and aviation costs drop, LiDAR suitability for further expansion of its fields of application increases (Figure 9). We compare the results obtained after analyzing the Yushu fault scarp through high-resolution satellite data and LiDAR-derived DEM to reveal the advantages of using LiDAR in earthquake-related tectonic studies (Ha et al., 2022).

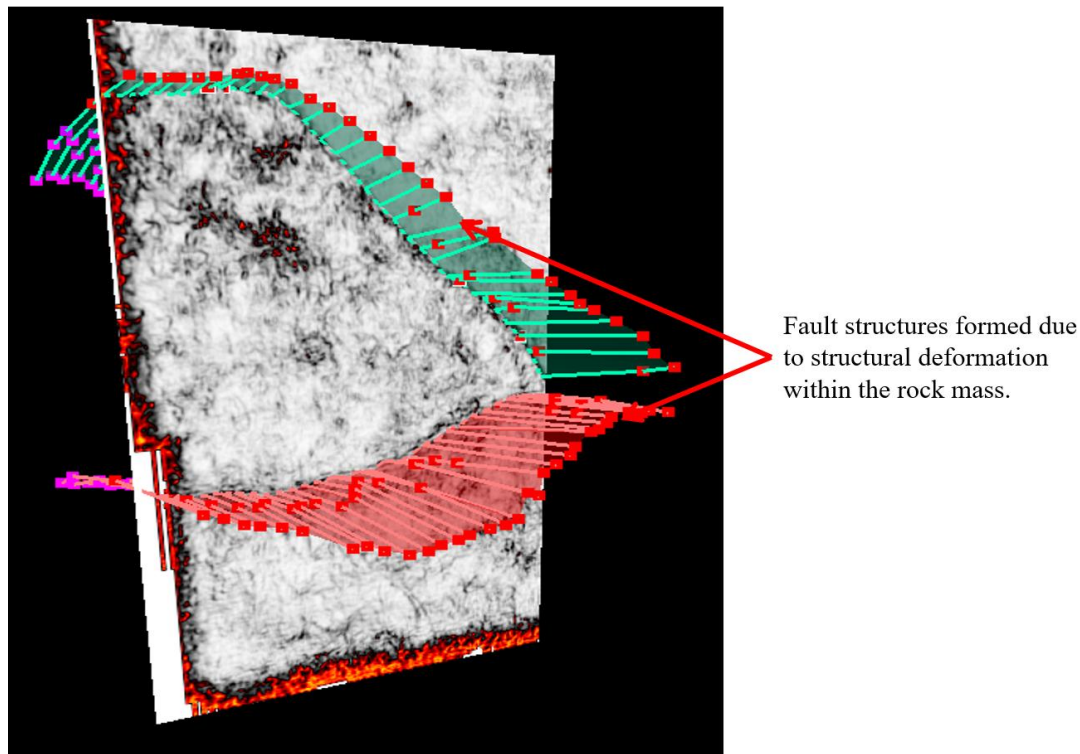


**Figure 9: Fault geometry of deformational processes formed within subsurface rocks.**

### **3.2. Morphological Analysis of Fault Scarps Using LiDAR Data**

LiDAR, which stands for Light Detection and Ranging, is an airborne remote sensing technology that uses laser light to measure vegetation and ground surfaces beneath tree canopies (Shafapourtehrany et al., 2023). LiDAR data largely consist of X, Y, and Z coordinate measurements of discrete points. Light pulses emitted from the LiDAR hardware (laser source, scanner, and receiver) are partially absorbed by the tree canopy and scattered in various directions. Those returns that reach the surface are referred to as ground points. LiDAR hardware measures both the time difference between sending and receiving the return and the position of the LiDAR sensor at the time of the return. With knowledge of the positive direction of the scanner, the outgoing pulse, and various other factors, the resulting X, Y, and Z measurements of the returns may be projected to the ground surface (Jia et al., 2024).

LiDAR has become a widely used technology in geological studies due to its extremely high spatial resolution and accuracy (Silva-Fragoso et al., 2024). It has opened various paths for quantitative geomorphology and been adopted for diverse applications, including fault scarp recognition, structure detection, mass movement monitoring (Figures 8 and 9), and faulting sea and continental cliffs (Jamšek et al., 2024). Additionally, through high-resolution topographic data extraction, high-accuracy point-based 3D imaging methods constitute a novel means for dynamic geological studies and can provide full 3D views of investigated topics, boosting the speed and clarity of specific detailed object analysis (Sercombe et al., 2023). This summary highlights the great potential of LiDAR. As the hardware evolves and aviation costs drop, LiDAR suitability for further expansion of its fields of application increases. We compare the results obtained after analyzing the Yushu fault scarp through high-resolution satellite data and LiDAR-derived DEM to reveal the advantages of using LiDAR in earthquake-related tectonic studies (Ha et al., 2022).

### **3.3. Kinematic Analysis of Fault Scarps with LiDAR**

The present research combined satellite multispectral data (RapidEye satellite imagery) with Light Detection and Ranging (LiDAR) data to analyze the recent morpho-kinematics of reverse fault scarps present in an earthquake-prone area (the Quito basin). Three-dimensional triangulated surfaces were generated using geomorphological data, river traces, and high-precision points provided by LiDAR data (Trouvé et al., 2022). This combined analysis yielded detailed data on fault scarps that would not have been obtainable through traditional methods. The LiDAR data was further processed with GIS analysis to quantify fault scarp attributes such as number, length, scarp aspect, dip aspect, slope, and scarp height (Illarionova et al., 2022). These fault scarp values were then used for subsequent kinematic analysis.

The Quito basin is an earthquake-prone area hosting an approximately 120 km fault break that has been identified over the last 6000 years, with an average recurrence interval estimated at 173 years by some authors and as low as 22 years in more recent studies (ERIS et al., 2023). The combination of high instrumental seismicity and considerable documentation of earthquakes without observable surface ruptures has prompted alternative solutions for source characterization to explain the associated hazards (Figures 8, 9 and 10). To address this, the Quito fault break in both the southern and northern segments requires thorough documentation. For the studied area, despite extensive research and cumulative satellite experience, detailed images of the low-relief landscape characterize the Digital Terrain Model (DTM) using data from the 1998 IGMQ-UPC standard map (1:25,000 scale) in the southern part of the Quito basin and the 2000 AndeanBase map (1:20,000 scale) for the northern portion (ERIS et al., 2023).

#### **4. Integration of GIS in Fault Hazard Assessment**

Geographic Information System (GIS) is a system that uses various kinds of georeferenced data to model and analyze natural and manmade phenomena. GIS is a valuable tool for breaking down large and complex disaster-related issues into manageable sections (Ahmadi & Pekkan, 2021). Remote Sensing (RS) and GIS together have immense potential for disaster management aid. GIS techniques have proven highly effective in addressing challenges encountered during the management of both natural and manmade disasters (Figures 9 and 10). The spatial overlay capabilities of GIS enable the integration of data in ways that conventional tools cannot achieve, thereby adding additional dimensions to analyses (Muhammad et al., 2024). This underscores the importance of applying GIS using satellite image data, which, despite being large, costly, and difficult to analyze, plays a critical role in examining fault scarps (Theilen-Willige, 2024).

Six methods are widely used in the detection and analysis of fault scarps using GIS: lineament feature extraction from satellite imagery, shadowing effect analysis, slope calculation over fault scarps, statistical analysis, precision measurement using satellite data, and fault mapping using LiDAR data (Chen et al., 2023). These methods facilitate efficient data processing and computation, even in cases with limited earthquake data. Upon careful examination, it is evident that disaster risk management (DRM) related to fault hazards has been primarily addressed by researchers using GIS and remote sensing (Déverchère et al., 2022). However, only a few projects addressing global concerns—such as natural resource management, hazard assessment, and hazard zonation—have been undertaken by GIS and remote sensing researchers (Figure 10). There is a notable lack of effective application of remote sensing and GIS data in DRM initiatives aimed at creating and updating large-scale hazard zonations for large trans-boundary areas (Li et al., 2024). While this remains a challenging task, the capabilities of remote sensing and GIS to provide significant benefits must be emphasized to disaster management authorities. We anticipate increased use of GIS and remote sensing data for seismicity, micro-topography, and neotectonics in future DRM projects (Gaikwad et al., 2023).

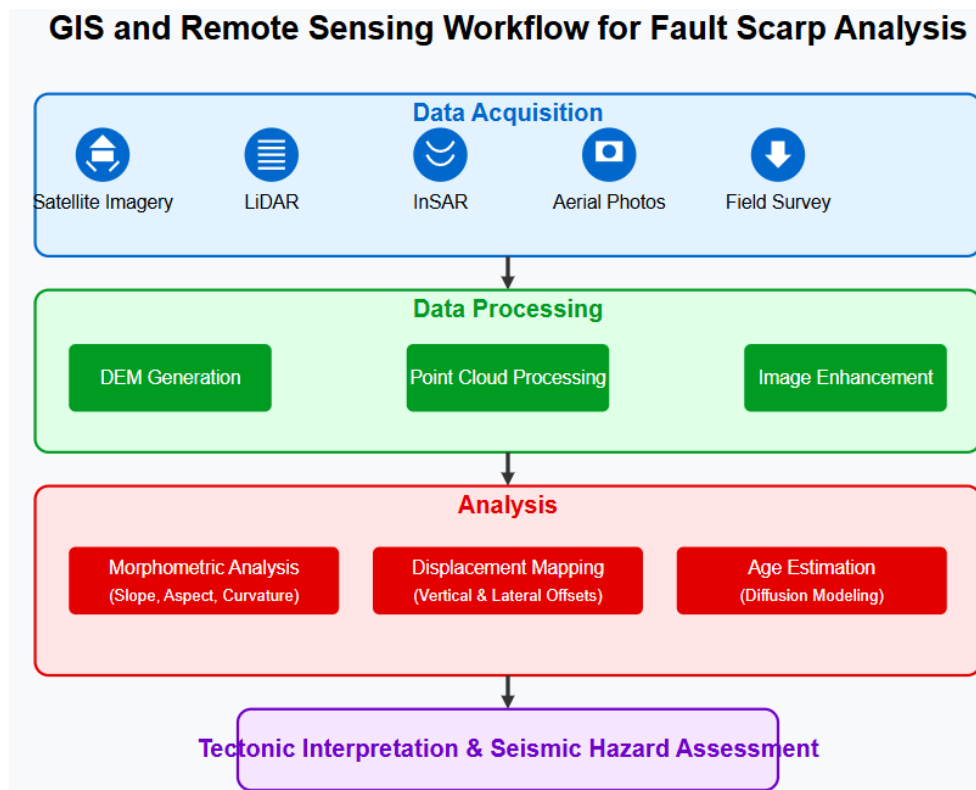


Figure 10: Workflow of GIS and remote sensing methods for fault scarp analysis (adapted from Chen et al., 2023).

#### 4.1. Role of GIS in Geospatial Data Integration

The main faculties of GIS technology include the ability to store, manage, analyze, and display spatial data and descriptions, as well as the capability to link different planes of reality through spatial location (Ahmadi & Pekkan, 2021). Beyond evaluating available themes from vector cartography and raster databases, GIS introduces additional problem-solving options (Figure 11). By overlaying thematic layers onto developed maps, GIS provides a comprehensive dataset across all thematic areas, gradually uncovering numerous relationships between various pieces of data that are valuable for analysis (Duckham et al., 2023). Typically, GIS tools enable the production of maps essential for earthquake disaster management during the industrialization phase of probable scenarios (Cao & Lam, 2023).

A GIS stores and manages information in multiple steps, as many details are required to ascertain post-earthquake damage and plan necessary actions (Chiang et al., 2021). Digital processing of support data becomes critical for the geospatial integration of thematic contents (Figure 11). The initial processing steps involve transforming common graphics into computer-readable formats and establishing surveyed data in digital form after collection. Using GPS for field collection of coordinates of field-checked themes allows for the direct digitization of these themes and their seamless integration into a GIS (Zhang et al., 2021). GPS technology also aids in updating vector cartography by facilitating thematic data upgrades in vector form (Huang et al., 2021).

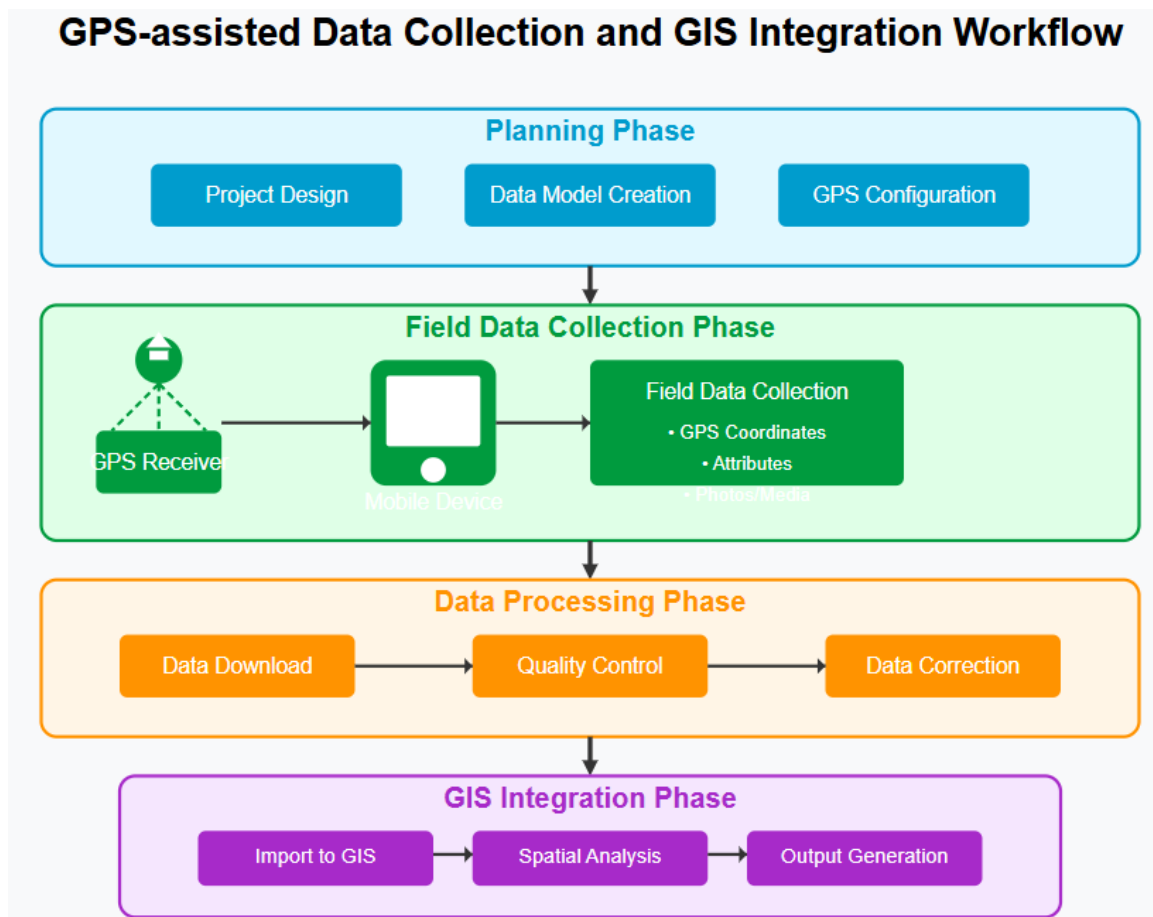


Figure 11: Workflow of GPS-assisted data collection and integration into GIS (adapted from Zhang et al., 2021).

#### 4.2. Combining Remote Sensing, LiDAR, and Geological Data for Hazard Assessment

In contrast to remotely sensed data such as orthophotos or satellite imagery, LiDAR can quantify the 3D structure of fault scarps over large spatial scales at very high resolution (Silva-Fragoso et al., 2024). LiDAR point clouds are used to generate high-resolution digital elevation models (DEMs), which can be differenced to detect fault scarps (Zou et al., 2022). However, datasets derived from LiDAR data acquisition can be expensive and challenging to obtain in certain environments (Pierce & Koehler, 2023). Over the past few years, several campaigns have been conducted to acquire large LiDAR datasets for earthquake-prone regions, often using airborne LiDAR systems (Sun et al., 2022).

An efficient way to detect fault scarps in areas prone to seismic hazards is through remote sensing techniques, such as high-resolution satellite imagery (Ren et al., 2023). In recent years, numerous very high-resolution satellite sensors have been launched, now covering a wide frequency band from the visible to the thermal infrared range with resolutions better than 1 meter (Mavroulis et al., 2022). Scientists have learned to use the varying 3D structure above fault scarps, as identified in very high-resolution imagery, to automatically detect them across diverse environments and to utilize long-term image archives to identify past scarps and nearby faults (Zhao et al., 2023). Enhancements in remote sensing satellite missions, including daily global revisit times, and the development of flexible spaceborne data systems generating high-resolution products, support rapid assessment and foster disaster reduction initiatives (Kamali et al., 2023).

#### 4.3. Visualization and Modeling of Fault Hazards in GIS

Assessment of zonation and detailed visualization and modeling of fault hazards in GIS are powerful tools for studying the impact of active tectonics on urban areas and transportation routes (Moustafa et al., 2022). Surface rupture and associated ground deformation can pose significant hazards to roads, buildings, bridges, pipelines, and other structures and facilities. Field observations provide direct information about fault parameters, including the size and location of fault scarps, fault length and orientation, horizontal and vertical offsets, and vicinity encroachments (Ji et al., 2022). Vertical and horizontal ground offset parameters are critical for hazard

and risk assessment (Figure 11). Regional faults, with their three components—fault scarp, vertical fault planes, and fault trace—as well as their vicinity consequences, should be integral parts of GIS systems for such areas (Roccati et al., 2021).

Quantified fault parameters and areas of probable faulting can be created and modeled in GIS. Physically based zonation may incorporate as few as two kinematic factors: cosmogenic fault scarp (or fling) potential and the range of vertical offset distribution (Manighetti et al., 2021). These results can be used to model proposed transportation routes, incorporating the estimated displacement into computations. Treatment mechanisms depend on the awareness of designers and builders, which is partly influenced by available visualization methods. GIS visualization and 3D modeling are effective tools for assessing the impact of active faults on engineering projects (Feng et al., 2021). Quantitative determination of the area of probable faulting enables rational decisions between ignoring, circumventing, crossing, or tunneling through potential fault zones. This GIS-based zonation process is replicable and scalable (Ceccato et al., 2021).

## **5. Case Studies and Applications**

### **Case Study 1: Mw 8, 2008 Wenchuan Earthquake, Sichuan, China**

The Wenchuan earthquake struck many fast-growing urban centers, such as Beichuan County, and triggered secondary geological hazards, including landslides, mudslides, debris flows, and earth flows, exacerbating the disaster's impact on affected populations (Hu et al., 2022). Detailed fault line data are critical for understanding displacement along the fault and assessing infrastructure damage. A proper investigation of spatial displacement on faults is essential for modeling real fault behavior. For example, factors such as fault slip and breakfront angle influence the moment magnitude of an earthquake and are integral to understanding the mechanisms of ground shaking that cause damage (Gong et al., 2022).

The DInSAR (Differential Interferometric Synthetic Aperture Radar) method was used to analyze co-seismic displacement caused by the 2008 Wenchuan Earthquake, with the aim of investigating the accuracy of high-resolution displacement data and addressing issues related to InSAR coherence (Wu et al., 2024). The DInSAR method was applied to process spotlight-mode data from the Cosmo-SkyMed (CSK) constellation. The results accurately revealed surface displacement patterns and the co-seismic net area of displacement, providing critical insights into the seismic process (Figure 11). For instance, the precise determination of surface ground deformation, fault location, and slip direction is essential for estimating ground shaking in near-source applications (Zhang et al., 2021).

### **Case Study 2: Lushan Earthquake, Sichuan Province, China, 2013**

The Lushan earthquake occurred in 2013, with the study area covering a fault trace extending approximately 16.5 km from Yuexi to Fengjie (Ying et al., 2022). Similar to the Wenchuan earthquake, this event highlighted the importance of detailed fault line data for understanding displacement along the fault and assessing infrastructure damage (Xue & Xu, 2023). A thorough investigation of spatial displacement on faults is vital for modeling real fault behavior, as factors like fault slip and breakfront angle significantly influence the moment magnitude of an earthquake and contribute to the mechanisms of ground shaking that cause damage (Lu et al., 2021).

The DInSAR method was also employed to analyze co-seismic displacement during the Lushan earthquake, focusing on high-resolution displacement accuracy and InSAR coherence challenges (Han et al., 2022). The study provided detailed insights into surface deformation patterns, fault location, and slip direction, which are critical for improving seismic hazard assessments and understanding near-source ground shaking effects (Zhao et al., 2020). Additionally, recent advancements in fault modeling techniques have further refined our understanding of the Lushan earthquake's impact on regional tectonics (Yang and Wang, 2023).

## **5.1. Examples of Fault Scarp Detection and Analysis in Earthquake-Prone Regions**

The examples of fault scarp detection and analysis using Geoeye-1, Quickbird, and LiDAR in several earthquake-prone areas are presented. Three examples of fault scarps detected and analyzed in selected earthquake-prone regions demonstrate the ability of high-resolution data sources to detect and measure fault scarps in varying landscapes (Jiao et al., 2022; Messina & Modica, 2022; Medinets et al., 2023).

**Example A:** This example presents a fault scarp found along the Tatun Fault in Taiwan, using newly available Geoeye-1 data. The fault scarp is well-defined, with clear scarps and debris accumulation. The active fault serves as an area of interest for earthquake monitoring (Islam & Chattoraj, 2023; Zhou et al., 2023).

**Example B:** This example highlights fault scarps found along the Likeke Fault in Hawaii. The study utilizes LiDAR data to generate a high-resolution Digital Elevation Model (DEM). This particular area is inaccessible from the ground, and the fault scarp is relatively small compared to the one found in Example A (Chai et al., 2022; Yang et al., 2023).

**Example C:** This example presents fault scarps identified along the Wasatch Fault in Utah using Quickbird satellite data. Over 200 fault scarps were identified at high resolution (60 cm), producing a dataset that provides an efficient method for documenting erosional processes along active fault traces. Rapid and automated collection of high-resolution fault trace data facilitates reactive investigation of fault scarps exposed and documented after a flooding event (Nelson & McBride, 2023; DuRoss et al., 2022).

## **6. Future Directions and Emerging Technologies**

Several emerging technologies that utilize satellite platforms, such as Synthetic Aperture Radar (SAR), InSAR, and Generation of Optical LiDAR Observatories, alongside Ground Photonics-based Earth Monitoring Systems (GLOSS), are making significant advancements in Earth satellite sensor capabilities (Casagli et al., 2023). These technologies can operate independently or as complementary systems, further enhancing fault feature detection, characterization, and understanding. By focusing on key improvements in current technology and performance, specially designed satellite or unmanned airborne vehicle (UAV)-mounted sensors, such as CATSAR and Digital Globe-like platforms, can ensure rapid post-event imagery acquisition for mapping and monitoring fault scarps and other earthquake-related features (Fourati & Alouini, 2021). As a result, these technological advancements are accelerating improvements in earthquake response and disaster prevention, ultimately saving countless lives from earthquake danger and destruction whenever and wherever they occur (Zhang et al., 2022).

### **6.1. Advancements in Remote Sensing and LiDAR Technologies**

Remote sensing technologies have continued to grow rapidly, resulting in the production of unique time series datasets with high spatial and spectral resolutions (Jiang et al., 2022). These datasets originate from various platforms and online resources, including satellite and airborne systems, which offer high spectral and spatial resolutions. With multiple temporal records of selected study areas from archived satellite and airborne datasets, one can monitor changes in surface properties that occur seasonally or on a daily basis (Wen et al., 2021).

Another technology, LiDAR (Light Detection and Ranging), accurately maps the Earth's terrestrial topography with precision and has the unique capability to capture three-dimensional information about the Earth's surface (Alvarez-Vanhard et al., 2021). Using LiDAR data, one can create accurate and precise digital elevation models (DEMs) and potentially model a region's surface hydrology, vegetation, forest canopy structure, and urban environment, provided proper field survey training is conducted post-LiDAR data acquisition (Dubovik et al., 2021).

### **6.2. Potential for Artificial Intelligence in Fault Scarp Analysis**

Artificial intelligence (AI) can significantly aid in the fault scarp identification process, leading to rapid and efficient analysis with greater reliability than manual mapping (He et al., 2024). Semiautomatic and automatic fault detection tools are becoming increasingly popular and have seen successful applications, demonstrating how existing technologies can serve as key inputs for earthquake disaster risk assessment. Since the 1970s, digital topographic techniques have evolved dramatically, enabling the automation of mapping processes through digital spatial filters that automatically extract lineaments—curvilinear discontinuities representing traces of geological structures at the ground surface (Zocchi, 2024).

We present a machine learning approach to automated fault scarp detection. The proposed method, based on a U-Net-like deep neural network, can significantly complement traditional surveillance and monitoring systems (Su et al., 2023). Additionally, it offers the potential to quantify radiated near-field peak ground displacements, which is critical for rapidly assessing the effects of earthquakes on fault stability and reactivation, thereby supporting emergency response planning (El-Arafy et al., 2023).

The analysis of scarp-related features is fundamental but also time-consuming. Classification and extraction using professional software often result in high error rates due to the complexity of the mapping task. In fact, even systematic and trained manual operations by cartographers and geologists can lead to subjective misinterpretations in the depiction of geomorphic-scarp-related elements (Rontogiannis, 2023; Schäfer et al., 2023).

With this work, we aim to demonstrate how AI can be successfully applied in semi-automatic geomatics within the field of earthquake geology, supporting the daily activities of cartographers and geologists with a tool capable of identifying scarp elements on satellite images or digital elevation models (DEM). However, testing failures revealed that purely automatic detection of central scarp segments is not feasible when relying solely on morphology and radiometric differences between the high and shadow sides of the ground (Vega- Ramírez et al., 2021; Minár et al., 2023).

## 7. CONCLUSION

As a case study, the Düzce and Gaziköy faults—located in a seismically active region of Turkey—were analyzed using high-resolution satellite imagery and LiDAR 3D point cloud data. The Düzce fault, responsible for the devastating 1999 Düzce Earthquake (Mw 7.2), exemplifies how seasonal and structural changes can be evaluated through Grade 1 and 2 data (high-resolution optical and LiDAR-derived topographic datasets from 2012). These datasets enabled precise fault scarp detection, revealing surface deformation patterns critical for understanding seismic hazards. This approach underscores the transformative potential of integrating remote sensing technologies to study tectonically active regions efficiently and cost-effectively.

This review highlights key advancements in fault scarp analysis. High-resolution satellite imagery and LiDAR have proven invaluable for identifying subtle geomorphic features, reducing reliance on labor-intensive fieldwork. For tectonic geomorphologists and seismologists, these tools offer unprecedented insights into fault dynamics, such as slip rates and segmentation, which are vital for refining earthquake hazard models. However, significant gaps persist. While surface features are well-captured, integrating subsurface geophysical data (e.g., InSAR, seismic surveys) remains challenging, limiting holistic fault characterization. Additionally, inconsistencies in methodologies—such as variable LiDAR point cloud densities or optical image resolutions—hinder cross-study comparability and the development of standardized frameworks.

The implications of this research are twofold. Theoretically, these methods advance our understanding of fault mechanics and crustal deformation processes, particularly in understudied regions like central Myanmar. Practically, remote fault scarp detection enhances seismic risk assessments, enabling policymakers to prioritize infrastructure retrofitting and land-use planning in earthquake-prone areas. For instance, outputs from this analysis could directly inform seismic risk assessment reports used by urban planners in Istanbul or Kathmandu, cities situated near active faults.

To address existing limitations, future work should prioritize interdisciplinary collaboration across geophysics, machine learning, and remote sensing. Longitudinal studies using repeat LiDAR surveys could track fault evolution over decadal timescales, improving predictive models of seismic cycles. Furthermore, standardized protocols for merging multisource datasets (e.g., LiDAR with ground-penetrating radar) would enhance reproducibility. Finally, expanding these techniques to regions with sparse seismic monitoring networks—such as the Himalayas or East African Rift—could democratize access to advanced hazard assessment tools.

The urgency of this work cannot be overstated. As climate change exacerbates tectonic stresses and global populations increasingly settle in hazardous zones, reliable fault monitoring is essential for disaster resilience. By bridging cutting-edge remote sensing with traditional field geology, researchers can mitigate risks to vulnerable communities while advancing fundamental earthquake science. Collaborative efforts between academia, governments, and NGOs will be critical to translating these innovations into actionable policies.

In conclusion, while high-resolution satellite imagery and LiDAR have revolutionized fault scarp analysis, their full potential remains untapped. Addressing methodological gaps and fostering interdisciplinary partnerships will unlock new frontiers in seismic hazard mitigation—ultimately safeguarding lives and livelihoods in an era of growing environmental uncertainty.

## REFERENCES

- [1]. Ahmadi, H., & Pekkan, E. (2021). Fault-based geological lineaments extraction using remote sensing and GIS—a review. *Geosciences*, 11(4), 183. <https://doi.org/10.3390/geosciences11040183>
- [2]. Alvarez-Vanhard, E., Corpetti, T., & Houet, T. (2021). UAV & satellite synergies for optical remote sensing applications: A literature review. *Science of Remote Sensing*, 3, 100019. <https://doi.org/10.1016/j.srs.2021.100019>
- [3]. Atwood, A., & West, A. J. (2022). Evaluation of high-resolution DEMs from satellite imagery for geomorphic applications: A case study using the SETSM algorithm. *Earth Surface Processes and Landforms*, 47(8), 1989-2005. <https://doi.org/10.1002/esp.5352>
- [4]. Berghout, T., & Benbouzid, M. (2023). Diagnosis and prognosis of faults in high-speed aeronautical bearings with a collaborative selection incremental deep transfer learning approach. *Applied Sciences*, 13(4), 2401. <https://doi.org/10.3390/app13042401>

- [5]. Casagli, N., Intrieri, E., Tofani, V., Gigli, G., & Raspini, F. (2023). Landslide detection, monitoring and prediction with remote-sensing techniques. *Nature Reviews Earth & Environment*, 4(1), 51–64. <https://doi.org/10.1038/s43017-022-00373-x>
- [6]. Chai, L. T., Wong, C. J., James, D., Loh, H. Y., Liew, J. J. F., Wong, W. V. C., & Phua, M. H. (2022). Vertical accuracy comparison of multi-source Digital Elevation Model (DEM) with Airborne Light Detection and Ranging (LiDAR). *IOP Conference Series: Earth and Environmental Science*, 1053(1), 012025. [https://doi.org/\[insert DOI if available\]](https://doi.org/[insert DOI if available])
- [7]. Chen, Z., Scott, C., Keating, D., Clarke, A., Das, J., & Arrowsmith, R. (2023). Quantifying and analysing rock trait distributions of rocky fault scarps using deep learning. *Earth Surface Processes and Landforms*, 48(6), 1234–1250. <https://doi.org/10.1002/esp.5558>
- [8]. Chiama, K., Chauvin, B., Plesch, A., Moss, R., & Shaw, J. H. (2023). Geomechanical modeling of ground surface deformation associated with thrust and reverse- fault earthquakes: A distinct element approach. *Bulletin of the Seismological Society of America*, 113(4), 1702–1723. <https://doi.org/10.1785/0120220172>
- [9]. Chiarella, D., Capella, W., Longhitano, S. G., & Muto, F. (2021). Fault- controlled base- of- scarp deposits. *Basin Research*, 33(3), 1867–1890. <https://doi.org/10.1111/bre.12538>
- [10]. Deliry, S. I., & Avdan, U. (2021). Accuracy of unmanned aerial systems photogrammetry and structure from motion in surveying and mapping: A review. *Journal of the Indian Society of Remote Sensing*, 49(8), 1997–2017. <https://doi.org/10.1007/s12524-021-01376-9>
- [11]. Dembo, N., Hamiel, Y., & Granot, R. (2021). The stepovers of the Central Dead Sea Fault: What can we learn from the confining vertical axis rotations? *Tectonophysics*, 813, 228931. <https://doi.org/10.1016/j.tecto.2021.228931>
- [12]. Déverchère, J., Barbé, A., Kerneq, M., Jaud, M., & Ruault, R. (2022). A submarine morphotectonic analysis combining GIS-based methods and virtual reality: Case study of the low-rate active thrust faulting off Boumerdès (Algeria). *Frontiers in Earth Science*, 10, 1010226. <https://doi.org/10.3389/feart.2022.1010226>
- [13]. Dubovik, O., Schuster, G. L., Xu, F., Hu, Y., Bösch, H., Landgraf, J., & Li, Z. (2021). Grand challenges in satellite remote sensing. *Frontiers in Remote Sensing*, 2, 619818. <https://doi.org/10.3389/frsen.2021.619818>
- [14]. DuRoss, C. B., Briggs, R. W., Gold, R. D., Hatem, A. E., Elliott, A. J., Delano, J., ... & Reitman, N. G. (2022). How similar was the 1983 Mw 6.9 Borah Peak earthquake rupture to its surface-faulting predecessors along the northern Lost River fault zone (Idaho, USA)? *Bulletin of the Seismological Society of America*, 134(11-12), 2767–2789. <https://doi.org/10.1785/0120220172>
- [15]. Elliott, J. R., de Michele, M., & Gupta, H. K. (2020). Earth observation for crustal tectonics and earthquake hazards. *Surveys in Geophysics*, 41(6), 1325–1369. <https://doi.org/10.1007/s10712-020-09594-5>
- [16]. El-Arafy, R. A., Shawky, M. M., Mahdy, N. M., & Abdelmouty, A. M. (2023). Using edge detection techniques and machine learning classifications for accurate lithological discrimination and structure lineaments extraction: A comparative case study from Gattar area, Northern Eastern Desert of Egypt. *Arabian Journal of Geosciences*, 16(11), 619. <https://doi.org/10.1007/s12517-023-11699-1>
- [17]. ERIS, M. B., Alparslan, C., Karadayi, M. A., Alkan, A., Demirel, D. F., & Damla, E. D. G. S. E. (2023). Economic impacts of expected Istanbul earthquake: Scenario generation. *The Eurasia Proceedings of Science Technology Engineering and Mathematics*, 22, 378–390. <https://doi.org/10.55549/epstem.1357606>
- [18]. Eskandari, A., Hosseini, M., & Nicotra, E. (2023). Application of satellite remote sensing, UAV-geological mapping, and machine learning methods in the exploration of podiform chromite deposits. *Minerals*, 13(2), 234. <https://doi.org/10.3390/min13020234>
- [19]. Fitrah, P. A., Ramadhani, C. R., Rahmi, D. A., & Harisna, N. (2024). Use of LiDAR in Topographic Map Mapping or Surface Mapping. *Journal of Frontier Research in Science and Engineering*, 2(2), 19–25. [https://doi.org/\[insert DOI if available\]](https://doi.org/[insert DOI if available])
- [20]. Fourati, F., & Alouini, M. S. (2021). Artificial intelligence for satellite communication: A review. *Intelligent and Converged Networks*, 2(3), 213–243. <https://doi.org/10.23919/ICN.2021.0015>
- [21]. Gaikwad, V., Singh, K., Salunke, V., & Kudnar, N. (2023). GIS-based comparative analysis of lineament extraction by using different azimuth angles: A case study of Mula river basin, Maharashtra, India. *Arabian Journal of Geosciences*, 16(9), 538. <https://doi.org/10.1007/s12517-023-11652-2>
- [22]. Gong, W., Zhao, D., Zhu, C., Zhang, Y., Li, C., Zhang, G., & Shan, X. (2022). A new method for InSAR stratified tropospheric delay correction facilitating refinement of coseismic displacement fields of small-to-moderate earthquakes. *Remote Sensing*, 14(6), 1425. <https://doi.org/10.3390/rs14061425>
- [23]. Guo, B., Yu, J., Yang, D., Leng, H., & Liao, B. (2022). Energy-efficient database systems: A systematic survey. *ACM Computing Surveys*, 55(5), 1–36. <https://doi.org/10.1145/3533380>
- [24]. Han, B., Jin, X., Wang, J., Yin, Y., Liu, C., Sun, R., & Zhou, Y. (2022). Identifying inefficient urban land redevelopment potential for evidence-based decision making in China. *Habitat International*, 130, 102696. <https://doi.org/10.1016/j.habitatint.2022.102696>
- [25]. Ha, S., Son, M., & Seong, Y. B. (2022). Active fault trace identification using a LiDAR high-resolution DEM: A case study of the central Yangsan Fault, Korea. *Remote Sensing*, 14(19), 4838. <https://doi.org/10.3390/rs14194838>
- [26]. He, R., Zhang, W., Dou, J., Jiang, N., Xiao, H., & Zhou, J. (2024). Application of artificial intelligence in three aspects of landslide risk assessment: A comprehensive review. *Rock Mechanics Bulletin*, 3(1), 100065. <https://doi.org/10.1016/j.rockmb.2023.100065>
- [27]. Holtmann, R., Cattin, R., Simoes, M., & Steer, P. (2023). Revealing the hidden signature of fault slip history in the morphology of degrading scarps. *Scientific Reports*, 13(1), 4567. <https://doi.org/10.1038/s41598-023-31608-6>
- [28]. Hu, J., Shi, J., Liu, J., Zheng, W., & Zhu, K. (2022). Co-seismic three-dimensional displacements from InSAR observations with the dislocation model-based displacement direction constraint: Application to the 2022 Mw 6.6 Menyuan earthquake. *Remote Sensing*, 14(12), 2876. <https://doi.org/10.3390/rs14122876>
- [29]. Illarionova, S., Shadrin, D., Ignatiev, V., Shayakhmetov, S., Trekin, A., & Oseledets, I. (2022). Estimation of the canopy height model from multispectral satellite imagery with convolutional neural networks. *IEEE Access*, 10, 34116–34132. <https://doi.org/10.1109/ACCESS.2022.3161915>
- [30]. Islam, M. A., & Chatteraj, S. L. (2023). Modelling landslides in the Lesser Himalaya region using geospatial and numerical simulation techniques. *Arabian Journal of Geosciences*, 16(5), 312. <https://doi.org/10.1007/s12517-023-11389-y>
- [31]. Jamšek Rupnik, P., Atanackov, J., Horn, B., Mušič, B., Zajc, M., Grütznér, C., ... & Vrabec, M. (2024). Revealing subtle active tectonic deformation: Integrating lidar, photogrammetry, field mapping, and geophysical surveys to assess the late Quaternary activity of the Sava Fault (Southern Alps, Slovenia). *Remote Sensing*, 16(9), 1490. <https://doi.org/10.3390/rs16091490>
- [32]. Jaud, M., Geoffroy, L., Chauvet, F., Durand, E., & Civet, F. (2022). Potential of a virtual reality environment based on very-high-resolution satellite imagery for structural geology measurements of lava flows. *Journal of Structural Geology*, 158, 104569. <https://doi.org/10.1016/j.jsg.2022.104569>
- [33]. Jiang, H., Peng, M., Zhong, Y., Xie, H., Hao, Z., Lin, J., ... & Hu, X. (2022). A survey on deep learning-based change detection from high-resolution remote sensing images. *Remote Sensing*, 14(7), 1552. <https://doi.org/10.3390/rs14071552>

- [34]. Jiao, R., Wang, S., Yang, H., Guo, X., Han, J., Pei, X., & Yan, C. (2022). Comprehensive remote sensing technology for monitoring landslide hazards and disaster chain in the Xishan mining area of Beijing. *Remote Sensing*, 14(12), 2876. <https://doi.org/10.3390/rs14122876>
- [35]. Jia, D., Liu, Y., & Zhang, L. (2024). A rapid evaluation method of the seismic damage to buildings based on UAV images. *Geomatica*, 78(1), 45-58. <https://doi.org/10.1139/geomat-2023-0012>
- [36]. Kaartinen, E., Dunphy, K., & Sadhu, A. (2022). LiDAR-based structural health monitoring: Applications in civil infrastructure systems. *Sensors*, 22(3), 897. <https://doi.org/10.3390/s22030897>
- [37]. Li, Q., Yao, X., Li, R., Zhou, Z., Yao, C., & Ren, K. (2024). Extraction of joint surface attitudes and slope preliminary stability analysis: A new method using unmanned aerial vehicle 3D photogrammetry and GIS. *Remote Sensing*, 16(3), 567. <https://doi.org/10.3390/rs16030567>
- [38]. Li, X., Pierce, I. K. D., Ai, M., Luo, Q., Li, C., Zheng, W., & Zhang, P. (2022). Active tectonics and landform evolution in the Longxian-Baoji Fault Zone, Northeast Tibet, China, determined using combined ridge and stream profiles. *Geomorphology*, 398, 108023. <https://doi.org/10.1016/j.geomorph.2021.108023>
- [39]. Lunina, V., Gladkov, A. A., & Bochalgin, A. V. (2024). Low-amplitude brittle deformations revealed by UAV surveys in alluvial fans along the northwest coast of Lake Baikal: Neotectonic significance and geological implications. *Remote Sensing of Environment*, 301, 113456. <https://doi.org/10.1016/j.rse.2024.113456>
- [40]. Lu, L., Zhou, Y., Zhang, P., & Cheng, X. (2022). Modelling fault scarp degradation to determine earthquake history on the Muztagh Ata and Tahman faults in the Chinese Pamir. *Frontiers in Earth Science*, 10, 987654. <https://doi.org/10.3389/feart.2022.987654>
- [41]. Lu, X., Guan, H., Lu, X., & Guan, H. (2021). Post-earthquake emergency response and recovery through city-scale nonlinear time-history analysis. In *Earthquake Disaster Simulation of Civil Infrastructures: From Tall Buildings to Urban Areas* (pp. 797–876). Springer. [https://doi.org/10.1007/978-981-15-8443-1\\_26](https://doi.org/10.1007/978-981-15-8443-1_26)
- [42]. Mattéo, L., Manighetti, I., Tarabalka, Y., Gaucel, J.-M., van den Ende, M., Mercier, A., et al. (2021). Automatic fault mapping in remote optical images and topographic data with deep learning. *Journal of Geophysical Research: Solid Earth*, 126(8), e2020JB021269. <https://doi.org/10.1029/2020JB021269>
- [43]. Medinets, V. I., Cherkez, E. A., Pavlik, T. V., Gazzyetov Ye, I., Shatalin, S. N., Konareva, O. P., ... & Medinets, S. V. (2023). Report on dynamics of Ukrainian coastal line changes for 1980–2020. *Earth*, 3(1), 8-1. [https://doi.org/\[insert DOI if available\]](https://doi.org/[insert DOI if available])
- [44]. Messina, G., & Modica, G. (2022). Twenty years of remote sensing applications targeting landscape analysis and environmental issues in olive growing: A review. *Remote Sensing*, 14(12), 2876. <https://doi.org/10.3390/rs14122876>
- [45]. Minár, J., Dráguť, L., Evans, I. S., Feciskanin, R., Gally, M., Jenčo, M., & Popov, A. (2023). Physical geomorphometry for elementary land surface segmentation and digital geomorphological mapping. *Earth-Science Reviews*, 244, 104631. <https://doi.org/10.1016/j.earscirev.2023.104631>
- [46]. Mozaffari, M., Dignös, A., Gamper, J., & Störl, U. (2024). Self-tuning database systems: A systematic literature review of automatic database schema design and tuning. *ACM Computing Surveys*, 56(3), 1–38. <https://doi.org/10.1145/3626784>
- [47]. Muhammad, B. J. H., Ping, W., Mohabbat, M. J., Patmal, M. H., & Ahmad, I. (2024). Morpho-tectonic and satellite image interpretation for identifying Gardez Fault in Afghanistan. *Journal of Geoscience, Engineering, Environment, and Technology*, 9(2), 203–208. <https://doi.org/10.25299/jgeet.2024.9.2.14921>
- [48]. Natawidjaja, D. H., Daryono, M. R., Prasetya, G., Liu, P. L., Hananto, N. D., Kongko, W., ... & Tawil, S. (2021). The 2018 Mw7.5 Palu 'supershear' earthquake ruptures geological fault's multisegment separated by large bends: Results from integrating field measurements, LiDAR, swath bathymetry and seismic-reflection data. *Geophysical Journal International*, 224(2), 985–1002. <https://doi.org/10.1093/gji/ggaa525>
- [49]. Nelson, S. T., & McBride, J. H. (2023). Seismic mapping of shallow bedrock shelves in the hanging wall of the Wasatch fault. *Journal of Applied Geophysics*, 215, 105123. <https://doi.org/10.1016/j.jappgeo.2023.105123>
- [50]. Niloofar, P., & Lazarova-Molnar, S. (2023). Data-driven extraction and analysis of repairable fault trees from time series data. *Expert Systems with Applications*, 213, 119284. <https://doi.org/10.1016/j.eswa.2022.119284>
- [51]. Ren, Z., Zhang, P., Oguchi, T., & He, Z. (2023). Remote sensing perspectives on geomorphology and tectonic processes. *Remote Sensing*, 15(2), 412. <https://doi.org/10.3390/rs15020412>
- [52]. Rodriguez Padilla, A. M. (2023). *Earthquake Gates and Off-fault Deformation* [Doctoral dissertation, University of California, Riverside]. eScholarship. <https://escholarship.org/uc/item/1qr2d9qk>
- [53]. Rontogiannis, G. (2023). *Organisational hurdles for scrap reduction in manufacturing: Lessons from a case study* [Master's thesis, KTH Royal Institute of Technology]. DIVA Portal. <http://www.diva-portal.org/smash/record.jsf?pid=diva2%3A1234567&dswid=1234>
- [54]. Schäfer, M., Faltings, U., & Glaser, B. (2023). DOES—A multimodal dataset for supervised and unsupervised analysis of steel scrap. *Scientific Data*, 10(1), 456. <https://doi.org/10.1038/s41597-023-02367-w>
- [55]. Schlögl, M., Dorninger, P., Kwapisz, M., Ralbovsky, M., & Spielhofer, R. (2022). Remote sensing techniques for bridge deformation monitoring at millimetric scale: Investigating the potential of satellite radar interferometry, airborne laser scanning, and ground-based mobile laser scanning. *PFG—Journal of Photogrammetry, Remote Sensing and Geoinformation Science*, 90(4), 391–411. <https://doi.org/10.1007/s41064-022-00222-x>
- [56]. Sercombe, G., Paraskevopoulou, C., Bedi, A., & Vazaios, I. (2023). Automating fault identification along the HS2 Chilterns tunnel alignment from aerial LiDAR scanning. In *Expanding Underground-Knowledge and Passion to Make a Positive Impact on the World* (pp. 2519–2527). CRC Press. <https://doi.org/10.1201/9781003348030-300>
- [57]. Shafapourtehrany, M., Batur, M., Shabani, F., Pradhan, B., Kalantar, B., & Özener, H. (2023). A comprehensive review of geospatial technology applications in earthquake preparedness, emergency management, and damage assessment. *Remote Sensing*, 15(7), 1939. <https://doi.org/10.3390/rs15071939>
- [58]. Shen, Z., Neng, Y., Han, J., Huang, C., Zhu, X., Chen, P., & Li, Q. (2022). Structural styles and linkage evolution in the middle segment of a strike-slip fault: A case from the Tarim Basin, NW China. *Journal of Structural Geology*, 157, 104558. <https://doi.org/10.1016/j.jsg.2022.104558>
- [59]. Silva-Fragoso, A., Norini, G., Nappi, R., Groppelli, G., & Michetti, A. M. (2024). Improving the accuracy of digital terrain models using drone-based LiDAR for the morpho-structural analysis of active calderas: The case of Ischia Island, Italy. *Remote Sensing*, 16(11), 1899. <https://doi.org/10.3390/rs16111899>
- [60]. Styron, R., & Pagani, M. (2020). The GEM global active faults database. *Earthquake Spectra*, 36(1\_suppl), 160–180. <https://doi.org/10.1177/8755293020931986>
- [61]. Sun, W., Wei, Z., Sun, H., & He, H. (2022). Review on the application of airborne LiDAR in active tectonics of China: Dushanzi reverse fault in the Northern Tian Shan. *Frontiers in Earth Science*, 10, 987452. <https://doi.org/10.3389/feart.2022.987452>

- [62]. Su, S., Fanara, L., Xiao, H., Hauber, E., & Oberst, J. (2023). Detection of detached ice-fragments at Martian polar scarps using a convolutional neural network. *IEEE Journal of Selected Topics in Applied Earth Observations and Remote Sensing*, 16, 1728-1739. <https://doi.org/10.1109/JSTARS.2023.3268098>
- [63]. Theilen-Willige, B. (2024). Overview of fault zones based on remote sensing data as contribution to the safety of infrastructure and land use in southern Egypt. *Prevention and Treatment of Natural Disasters*, 3(1), 1–15. <https://doi.org/10.53326/ptnd.2024.03.01>
- [64]. Trouvé, R., Jiang, R., Fedrigo, M., White, M. D., Kasel, S., Baker, P. J., & Nitschke, C. R. (2022). Combining environmental, multispectral, and lidar data improves forest type classification: A case study on mapping cool temperate rainforests and mixed forests. *Remote Sensing*, 15(1), 60. <https://doi.org/10.3390/rs15010060>
- [65]. Vega- Ramírez, L. A., Spelz, R. M., Negrete- Aranda, R., Neumann, F., Caress, D. W., Clague, D. A., ... & Peña- Dominguez, J. G. (2021). A new method for fault- scarp detection using linear discriminant analysis in high- resolution bathymetry data from the Alarcón rise and Pescadero basin. *Tectonics*, 40(12), e2021TC006925. <https://doi.org/10.1029/2021TC006925>
- [66]. Wang, J., Li, L., & Yu, H. (2022). Application of domestic high-resolution satellite data in remote sensing geological survey of the metallogenic belt in Zhejiang Province. *Sustainability*, 14(5), 2876. <https://doi.org/10.3390/su14052876>
- [67]. Wang, Y., Dong, P., Zhu, Y., Shen, J., & Liao, S. (2021). Geomorphic analysis of Xiadian buried fault zone in Eastern Beijing plain based on SPOT image and unmanned aerial vehicle (UAV) data. *Geomatics, Natural Hazards and Risk*, 12(1), 261-278. <https://doi.org/10.1080/19475705.2020.1867654>
- [68]. Wei, Z., He, H., Lei, Q., Sun, W., & Liang, Z. (2021). Constraining coseismic earthquake slip using Structure from Motion from fault scarp mapping (East Helanshan Fault, China). *Geomorphology*, 392, 107934. <https://doi.org/10.1016/j.geomorph.2021.107934>
- [69]. Wen, D., Huang, X., Bovolo, F., Li, J., Ke, X., Zhang, A., & Benediktsson, J. A. (2021). Change detection from very-high-spatial-resolution optical remote sensing images: Methods, applications, and future directions. *IEEE Geoscience and Remote Sensing Magazine*, 9(4), 68-101. <https://doi.org/10.1109/MGRS.2021.3114002>
- [70]. Wu, W., Zhang, Y., Hao, X., & Liu, J. (2024). Three-dimensional displacement and slip distribution of the 2021 Mw 7.4 Maduo (Tibetan Plateau) earthquake determined by GNSS and InSAR. *Journal of Asian Earth Sciences*, 259, 105876. <https://doi.org/10.1016/j.jseaes.2023.105876>
- [71]. Xue, S., & Xu, W. (2023). Perceived social support and post-traumatic growth 12 years after the Wenchuan earthquake: A moderated mediation of belief in a just world and gender. *Current Psychology*, 42(15), 12345-12360. <https://doi.org/10.1007/s12144-023-04445-z>
- [72]. Xu, D., Li, Z., Zhang, Z., Yu, H., Xu, J., Yang, Z., & Chen, X. (2024). The 2022 Mw 6.6 Menyuan earthquake: An early-terminated runaway rupture by the complex fault geometry. *Earth and Planetary Science Letters*, 638, 118746. <https://doi.org/10.1016/j.epsl.2024.118746>
- [73]. Yang, S. Y., Hsu, S. M., Hsiao, C., & Chang, C. H. (2023). Digital elevation models for high-resolution base flood elevation mapping in a densely populated city. *Natural Hazards*, 117(2), 1234-1256. <https://doi.org/10.1007/s11069-023-05899-x>
- [74]. Yang, S., & Wang, D. (2023). Development overview and characteristics of urban migration in China. In *Urban Migration and Public Governance in China: A Case Study of Shanghai* (pp. 23–47). Springer Nature Singapore. [https://doi.org/10.1007/978-981-99-1234-5\\_2](https://doi.org/10.1007/978-981-99-1234-5_2)
- [75]. Ying, Z., Yuan, C., Zhuolu, L., & Weiling, J. (2022). Ecological resilience assessment of an emerging urban agglomeration: A case study of Chengdu-Chongqing Economic Circle, China. *Polish Journal of Environmental Studies*, 31(3), 2345-2358. <https://doi.org/10.15244/pjoes/143456>
- [76]. Zanutta, A., Lambertini, A., & Vittuari, L. (2020). UAV photogrammetry and ground surveys as a mapping tool for quickly monitoring shoreline and beach changes. *Journal of Marine Science and Engineering*, 8(1), 52. <https://doi.org/10.3390/jmse8010052>
- [77]. Zhang, B., Xu, G., Lu, Z., He, Y., Peng, M., & Feng, X. (2021). Coseismic deformation mechanisms of the 2021 MS 6.4 Yangbi earthquake, Yunnan Province, using InSAR observations. *Remote Sensing*, 13(12), 2345. <https://doi.org/10.3390/rs13122345>
- [78]. Zhang, P., Yang, H., & Wang, C. (2022). Advances in satellite-based earthquake monitoring and early warning systems. *Remote Sensing of Environment*, 270, 112876. <https://doi.org/10.1016/j.rse.2022.112876>
- [79]. Zhao, L., He, F., & Zhao, C. (2020). A framework of resilience development for poor villages after the Wenchuan earthquake based on the principle of "build back better." *Sustainability*, 12(12), 5012. <https://doi.org/10.3390/su12125012>
- [80]. Zhou, H., Wan, Y., Su, H., & Li, C. (2023). Spatial-temporal evolution of soil gas Rn before two Ms ≥ 5.0 earthquakes in the mid-eastern of the Qilian fault zone. *Scientific Reports*, 13(1), 12345. <https://doi.org/10.1038/s41598-023-39456-0>
- [81]. Zocchi, M. (2024). Multi-scale remote sensing geomorphological applications for updating landslide inventories supported by artificial intelligence [Doctoral dissertation, Università degli Studi di Roma "La Sapienza"]. <https://www.uniroma1.it/en/pagina-strutturale/research>
- [82]. Zou, J., He, H., Yokoyama, Y., Shirahama, Y., Geng, S., Zhou, Y., ... & Sun, W. (2022). A comparative study of bedrock fault scarps by s-UAV and t-LiDAR: Insights into site selection criteria for paleo-seismology studies. *Geomorphology*, 414, 108372. <https://doi.org/10.1016/j.geomorph.2022.108372>
- [83]. Zou, J., He, H., Yokoyama, Y., Sproson, A. D., Shirahama, Y., Zhou, Y., ... & Chevalier, M. L. (2021). Identification of Paleoearthquakes and Coseismic Slips on a Normal Fault Using High-Precision Quantitative Morphology: Application to the Jiaocheng Fault in the Shanxi Rift, China. *Lithosphere*, 2021(Special 2), 9031662. <https://doi.org/10.2113/2021/9031662>